

Effect of Mn content on the structure and electrochemical characteristics of $\text{La}_{0.7}\text{Mg}_{0.3}\text{Ni}_{2.975-x}\text{Co}_{0.525}\text{Mn}_x$ ($x = 0-0.4$) hydrogen storage alloys

X.B. Zhang^a, D.Z. Sun^b, W.Y. Yin^a, Y.J. Chai^a, M.S. Zhao^{a,*}

^a Key Laboratory of Rare Earth Chemistry and Physics, Changchun Institute of Applied Chemistry, Graduate School of Chinese Academy of Sciences, Chinese Academy of Sciences, Changchun 130022, PR China

^b State Key Laboratory of Electro-analytical Chemistry, Changchun Institute of Applied Chemistry, Graduate School of Chinese Academy of Sciences, Chinese Academy of Sciences, Changchun 130022, PR China

Received 2 November 2004; received in revised form 15 November 2004; accepted 15 November 2004

Available online 25 December 2004

Abstract

The effect of Mn content on the crystal structure and electrochemical characteristics of $\text{La}_{0.7}\text{Mg}_{0.3}\text{Ni}_{2.975-x}\text{Co}_{0.525}\text{Mn}_x$ ($x = 0, 0.1, 0.2, 0.3, 0.4$) alloys has been studied systematically. The results of the Rietveld analyses show that all these alloys mainly consist of two phases: the $\text{La}(\text{La},\text{Mg})_2\text{Ni}_9$ phase with the rhombohedral PuNi_3 -type structure and the LaNi_5 phase with the hexagonal CaCu_5 -type structure. The pressure–composition isotherms shows that the partial substitution of Mn for Ni results in lower desorption plateau pressure and steeper pressure plateau of the alloy electrodes. For a Mn content of $x = 0.3$, the electrochemical performances, including specific discharge capacity, high rate chargeability (HRC) and high rate dischargeability (HRD), of the alloy are preferable. Moreover, the data of the polarization resistance R_p and the exchange current density I_0 of the alloy electrodes is consistent with the results of HRC and HRD. The hydrogen diffusion coefficient D increases with increasing Mn content, and thereafter increases the low temperature dischargeability (LTD) of the alloy electrodes.

© 2004 Elsevier Ltd. All rights reserved.

Keywords: Structure characteristics; High rate chargeability; High rate dischargeability; Low temperature dischargeability; Exchange current density; Hydrogen diffusion coefficient

1. Introduction

Owing to the shortage of fossil energy and global warming, hydrogen is expected to be a promising energy carrier in near future. In order for hydrogen to become a viable solution to the energy crisis and the environmental problems, storage processes must be improved in terms of specific capacity and security. Among different ways to store hydrogen, absorption in solid is very attractive since it allows safe storage at pressure and temperature close to ambient conditions [1]. There are many kinds of metals and alloys which are able to absorb large quantity of hydrogen, and they are used in many fields, such as

heat pump, thermal storage system, as catalysts, fuel cells, nickel–metal hydride (Ni–MH) rechargeable batteries and so on.

In recent years, Ni–MH secondary battery, in which hydrogen storage alloy is employed as negative electrode material, has been widely adopted in various portable electronic devices, electric hand tools and electric vehicles because of its high reversible energy storage density, fast electrochemical activation, long cyclic life, good charge/discharge kinetics and environmental compatibility [2–7]. Nowadays, two kinds of metal–hydride alloys, namely the rare earth-based AB_5 type and the Zr-based AB_2 type alloys, especially the former, have been widely commercialized in the nickel metal–hydride (Ni–MH) battery industry. However, AB_5 alloys are now not very satisfactory due to their limited discharge capacity (about 372 mAh g^{-1}) [8]. Moreover,

* Corresponding author. Tel.: +86 431 5262365; fax: +86 431 5685653.
E-mail address: zhaoms@ciac.jl.cn (M.S. Zhao).

although the Zr-based AB₂-type alloys have a higher specific energy than that of the AB₅ alloys [9], they have the demerits of slow activation, higher cost and poor high rate dischargeability [10]. Therefore, alloys with higher energy density, faster activation and lower cost are urgently to be found to replace the conventional rare earth-based AB₅-type alloys. Oesterreicher et al. [11,12] pointed out that the hydrogen storage capacity of LaNi₃ and CaNi₃ alloys exceeds that of the well-known LaNi₅ alloy. They also indicated that the LaNi₃ and CaNi₃ could react rapidly with hydrogen under ambient conditions to form LaNi₃H₅ and CaNi₃H_{4.6}, respectively. Recently, Kadir et al. [13–15] have discovered a new type of ternary alloys with the general formula of RMg₂Ni₉ (R: rare earth, Ca, Y) with PuNi₃ type structure. It is found that some of the R–Mg–Ni based ternary alloys can absorb–desorb 1.8–1.87 mass% H₂ and are thus regarded as promising candidates for reversible gaseous hydrogen storage [16,17]. As to their electrochemical hydrogen storage, Pan et al. [18] have reported that the discharge capacity of La_{0.7}Mg_{0.3}Ni_{2.975}Co_{0.525} alloy reaches 398.4 mAh g⁻¹, which is very attractive for practical application. However, the La–Mg–Ni–Co system hydrogen storage electrode alloys have some disadvantages, such as a high absorption/desorption plateau pressure, poor cyclic stability and so on. It is well known that elemental substitution is one of the most effective methods for improving the overall properties of the hydrogen storage alloys and obtaining the desired overall properties, e.g. proper capacity at a favorable hydrogen pressure, favorable HRD and good cyclic stability [19–22]. For rare earth-based hydrogen storage alloys, partial substitution of Ni by elements such as Al [19], Mn [20], Cu [21], Sn [22] and Fe [23] has been widely studied. Several metals have turned out to be good candidates for lowering the plateau pressure [19,20]. It has been found that the Mn element is beneficial to many aspects for rare earth-based hydrogen storage alloys [24–27]. Sakai et al. [26] pointed out that the maximum discharge capacity of the LaNi_{4.5}Mn_{0.5} alloy electrode reaches 318 mAh g⁻¹. Ogawa and Ikoma [27] have studied the hydrogen storage property and electrochemical characteristics of the MnNi_{3.95–x}Mn_xAl_{0.3}Co_{0.75} electrode alloys and indicated that the equilibrium pressure decreased from 0.24 to 0.083 MPa with increasing *x* from 0.2 to 0.4, and the activity, discharge capacity and high rate dischargeability of the alloy electrodes can be improved. In addition, previous researches indicated that the partial substitution of Mn for Ni can increase the lattice parameters and the cell volume, decrease the plateau equilibrium pressure and improve electrochemical catalytic activity of alloys [28]. Therefore, it is believed that partial substitution of Mn for Ni will be a very effective way to improve the overall properties of the La–Mg–Ni–Co system hydrogen storage alloys.

In this paper, we focus on the detailed influence of partial substitution for Ni with Mn on the structural and electrochemical characteristics of the La_{0.7}Mg_{0.3}Ni_{2.975–x}Co_{0.525}Mn_x (*x* = 0–0.4) hydrogen storage alloys.

2. Experimental details

2.1. Alloy preparation and X-ray diffraction analysis

All alloy samples were prepared by arc-melting carefully the constituent elements or master alloy on a water-cooled copper hearth under the protection of argon atmosphere. The purity of the metals, i.e., La, Mg, Ni, Co and Mn is higher than 99.9 mass%, respectively. The samples were all turned over and remelted five times to ensure good homogeneity. A slight excess of Mg over composition was needed in order to compensate for evaporative loss of Mg under preparation conditions. Several attempts were done until the optimum preparative conditions were found. The final compounds were carefully checked by Inductively Coupled Plasma–Atomic Emission Spectrometry (ICP–AES) method using TJA Poems-type instrument. Thereafter, these alloy samples were mechanically crushed to particle with an average diameter of 26.24 μm (300 mesh).

Crystallographic characteristics of the hydrogen storage alloys were investigated by X-ray diffraction on Rigaku D/Max 2500PC X-ray diffractometer (Cu Kα radiation, Bragg–Brentano geometry, 2θ range 10–100°, step size 0.02°, backscattered rear graphite monochromator). The lattice constants and cell volume were calculated by Rietica program [29] after internal theta calibration using silicon as standard reference materials.

2.2. Electrochemical measurement

The preparation of the disk-type electrodes, the setup of the electrochemical cell and the measurement of electrochemical properties were similar as described in our previous paper [30].

Pressure–composition isotherms (*P–C–T*) curves were electrochemically obtained by converting the equilibrium potential of the metal hydride electrode to the equilibrium pressure of hydrogen on the basis of Nernst equation using electrochemical data [31] as reported in reference [32]. The equilibrium potential curves were obtained by alternating the following two processes: (1) a pulse discharge of (25 mA g⁻¹ × 0.25 h) and (2) a rest period until the potential became almost constant. The equilibrium potential change of approximately 30 mV corresponds to the equilibrium pressure change by one order of magnitude. Since the measured potentials have an error of 1–2 mV, the calculated pressure values are accurate to be within 10% [31].

To evaluate the HRD (in the range of 60–1200 mA g⁻¹), the charging current density was kept constant at 60 mA g⁻¹ and the obtained discharge capacity was denoted as *C_i*. On the other hand, when the HRC (60–1200 mA g⁻¹) was investigated, the discharging current density was held at 60 mA g⁻¹ and thus we got the discharge capacity (*C_j*). HRD (or HRC) are generally defined as the ratio of the discharge capacity *C_i* (or *C_j*) at the cut off voltage of –0.6 V to the

maximum capacity C_{\max} , namely: $\text{HRD} = C_i/C_{\max} \times 100\%$, $\text{HRC} = C_j/C_{\max} \times 100\%$, respectively.

For investigating the electrocatalytic activity of the hydrogen electrode reaction, the linear polarization curves of the electrode were plotted on a EG&G PARC's Model 273 Potentiostat/Galvanostat station by scanning the electrode potential at the rate of 0.1 mV s^{-1} from -5 to 5 mV (versus open circuit potential) at 50% depth of discharge (DOD) at 298 and 233 K, respectively. The polarization resistance, R_p , can be obtained from the slope of the linear polarization curves. Moreover, the exchange current density, I_0 , which is a measure of the catalytic activity of electrode, was calculated from the slopes of polarization curves by the following equation [33],

$$I_0 = \frac{RT}{FR_p}$$

where R , T and F have their general meanings and R_p is the polarization resistance. The potentiostatic discharge technique was used to evaluate the coefficient of diffusion within the bulk of the alloy electrodes. After being fully charged followed by a 30 min open-circuit lay-aside, the electrodes were discharged with $+500 \text{ mV}$ potential-step for 500 s on a EG&G PARC's Model 273 Potentiostat/Galvanostat station, using the M352 CorrWare electrochemical/corrosion software.

3. Results and discussion

3.1. Alloy composition and structure characteristic

It is well known that the low melting Mg metal will be inevitably lost during the sample preparation. We have tried many ways to overcome this problem, such as using Mg–Ni master alloy as Mg additive, decreasing the melting current, adding a slight excess of Mg over sample composition and so on. The third way is the most effective way to compensate for evaporative loss of Mg among all these methods mentioned above. The loss of Mg should be seriously paid in the alloy preparation process, whereas no compensation on Mg loss is described in Pan et al.'s paper [33]. In present paper, the lost weight during sample preparation is about 0.5 mass%, which is almost the same as excess Mg added. The results of ICP–AES analysis for all compounds are summarized in Table 1. It can be seen that the final composition of all the alloys is identical with the original composition.

Fig. 1 shows the result of Rietveld refinement of XRD profiles for $\text{La}_{0.7}\text{Mg}_{0.3}\text{Ni}_{2.875}\text{Co}_{0.525}\text{Mn}_{0.1}$ hydrogen storage alloy as a representative example of $\text{La}_{0.7}\text{Mg}_{0.3}\text{Ni}_{2.975-x}\text{Co}_{0.525}\text{Mn}_x$ ($x=0, 0.1, 0.2, 0.3, 0.4$) hydrogen storage alloys. The result shows that the $\text{La}_{0.7}\text{Mg}_{0.3}\text{Ni}_{2.875}\text{Co}_{0.525}\text{Mn}_{0.1}$ alloy consists of two phases: a La_2MgNi_9 phase with a PuNi_3 -type rhombohedral structure and a LaNi_5 phase with a CaCu_5 -type hexagonal structure. The final Rietveld structure parameters are tabulated in

Table 1
Composition of the $\text{La}_{0.7}\text{Mg}_{0.3}\text{Ni}_{2.975-x}\text{Co}_{0.525}\text{Mn}_x$ ($x=0, 0.1, 0.2, 0.3, 0.4$) alloys

Samples	La (mg g^{-1})	Mg (mg g^{-1})	Ni (mg g^{-1})	Co (mg g^{-1})	Mn (mg g^{-1})	La:Mg:Ni:Co:Mn ^a
$\text{La}_{0.7}\text{Mg}_{0.3}\text{Ni}_{2.975}\text{Co}_{0.525}$	313.57	23.52	563.14	99.77	0.00	2.26:0.97:9.59:1.69
$\text{La}_{0.7}\text{Mg}_{0.3}\text{Ni}_{2.875}\text{Co}_{0.525}\text{Mn}_{0.1}$	313.95	23.55	544.87	99.89	17.74	2.26:0.97:9.28:1.70:0.32
$\text{La}_{0.7}\text{Mg}_{0.3}\text{Ni}_{2.775}\text{Co}_{0.525}\text{Mn}_{0.2}$	314.33	23.58	526.56	100.01	35.52	2.26:0.97:8.97:1.70:0.65
$\text{La}_{0.7}\text{Mg}_{0.3}\text{Ni}_{2.675}\text{Co}_{0.525}\text{Mn}_{0.3}$	314.71	23.60	508.22	100.13	53.34	2.27:0.97:8.66:1.70:0.97
$\text{La}_{0.7}\text{Mg}_{0.3}\text{Ni}_{2.575}\text{Co}_{0.525}\text{Mn}_{0.4}$	315.09	23.63	489.82	100.25	71.21	2.27:0.97:8.34:1.70:1.30

^a Atomic ratio.

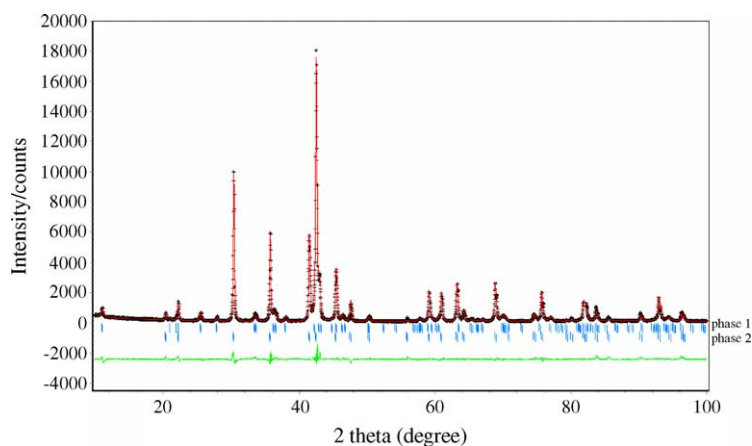


Fig. 1. Rietveld profiles refinement of XRD patterns $\text{La}_{0.7}\text{Mg}_{0.3}\text{Ni}_{2.875}\text{Co}_{0.525}\text{Mn}_{0.1}$ alloy (phase 1: $\text{La}(\text{La},\text{Mg})_2\text{Ni}_9$; phase 2: LaNi_5).

Table 2

Crystallographic parameters for La_2MgNi_9 by using X-ray diffraction $\text{Cu K}\alpha$ ($\lambda = 1.5405981 \text{ \AA}$) at 298 K in a space group $R\bar{3}m$ and $Z = 3^a$

Atom	Site	Metal atom position			Occupancy
		x	y	z	
La1	3a	0	0	0	1
La2	6c	0	0	0.14749(17)	0.484
Mg1	6c	0	0	0.14749(17)	0.516
Ni1	6c	0	0	0.32563(11)	1
Ni2	3b	0	0	0.5	1
Ni3	18h	0.4947(2)	0.5054(8)	0.08333(12)	1

^a Structure was refined by using the Rietveld refinement program Rietica. The pattern factor $R_p = 5.6$, the weighted pattern factor $R_{wp} = 7.5$ and the goodness of fit $S = 1.8$.

Table 2. The crystallographic results reveal that the Mg atoms only occupy the 6c sites whereas the La atoms can occupy both the 3a and the 6c sites in the phase with rhombohedral (Space group: $R\bar{3}m$ 166) PuNi_3 -type structure by Rietveld refinement. So the final formula of La_2MgNi_9 phase can be designated as $\text{La}(\text{La},\text{Mg})_2\text{Ni}_9$. The lattice parameters and cell volumes of the phases of the hydrogen storage alloys are listed in Table 3. We can find that all the alloys mainly consisted of two crystallographic phases, namely the $\text{La}(\text{La},\text{Mg})_2\text{Ni}_9$ phase and the LaNi_5 phase. Fig. 2 shows the lattice parameters and unit cell volumes of the alloys as a function of x . It can be seen that a and c parameters of both the $\text{La}(\text{La},\text{Mg})_2\text{Ni}_9$ phase and the LaNi_5 phase in the alloys all increase linearly with increasing Mn content, which is mainly ascribed to the larger atomic radius of Mn (1.79 Å) than that of Ni (1.62 Å). The Fig. 3 shows the abundances of the $\text{La}(\text{La},\text{Mg})_2\text{Ni}_9$ phase and the LaNi_5 phase as a function of Mn content in the alloys. It can be seen that the $\text{La}(\text{La},\text{Mg})_2\text{Ni}_9$ phase abundance decrease from 71.32 to 60.35% with increasing x , on the contrary, the LaNi_5 phase abundance increases from 28.68 to 39.65%. The above results are somewhat different to those obtained by Pan et al. For instance, there are no existences of MnO_2 phase in our experiment, and the phase abundances of LaNi_5 phase and $\text{La}(\text{La},\text{Mg})_2\text{Ni}_9$ phase are different to their results. It is well known that all La–Mg–Ni–Co–Mn

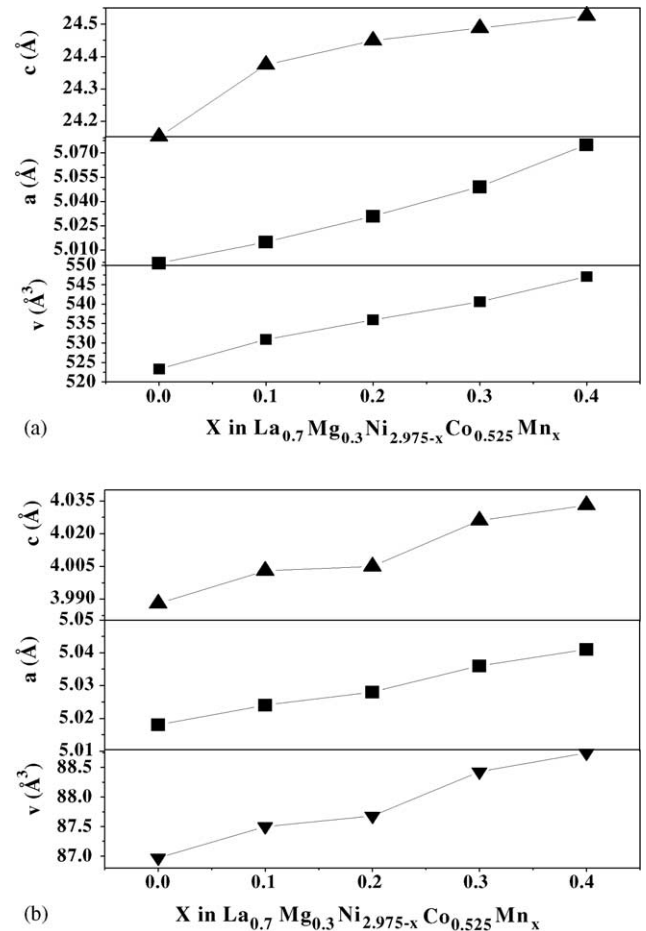


Fig. 2. The lattice parameters and cell volume of the $\text{La}_{0.7}\text{Mg}_{0.3}\text{Ni}_{2.975-x}\text{Co}_{0.525}\text{Mn}_x$ ($x = 0-0.4$) alloys (a) $\text{La}(\text{La},\text{Mg})_2\text{Ni}_9$ phase and (b) LaNi_5 phase.

system hydrogen storage alloys are of multiphase and different preparation conditions will result in different phase abundance. Magnetic levitation melting and arc-melting method are used in Pan et al.'s and our experiments, respectively. Those two preparation methods would be responsible for the

Table 3

The characteristics of alloy phases in $\text{La}_{0.7}\text{Mg}_{0.3}\text{Ni}_{2.975-x}\text{Co}_{0.525}\text{Mn}_x$ ($x = 0-0.4$) alloys^a

Samples	Phases	Phase abundance (wt.%)	Parameters of fit ^b	Lattice parameter (Å)		Cell volume (Å ³)
				a	c	
$x = 0.0$	$\text{La}(\text{La},\text{Mg})_2\text{Ni}_9$	71.32	$R_p = 8.7$	5.002	24.153	523.35
	LaNi_5	28.68	$R_{wp} = 11.4$	5.018	3.988	86.97
$x = 0.1$	$\text{La}(\text{La},\text{Mg})_2\text{Ni}_9$	69.21	$R_p = 9.7$	5.015	24.375	530.91
	LaNi_5	30.79	$R_{wp} = 13.1$	5.024	4.003	87.5
$x = 0.2$	$\text{La}(\text{La},\text{Mg})_2\text{Ni}_9$	67.53	$R_p = 8.6$	5.031	24.450	535.94
	LaNi_5	32.47	$R_{wp} = 11.3$	5.028	4.005	87.68
$x = 0.3$	$\text{La}(\text{La},\text{Mg})_2\text{Ni}_9$	64.16	$R_p = 6.3$	5.049	24.488	540.62
	LaNi_5	35.84	$R_{wp} = 8.5$	5.036	4.026	88.43
$x = 0.4$	$\text{La}(\text{La},\text{Mg})_2\text{Ni}_9$	60.35	$R_p = 8.6$	5.075	24.526	547.05
	LaNi_5	39.65	$R_{wp} = 11.3$	5.041	4.033	88.75

^a The Rietveld refinement program RIETICA was used.

^b R_p : the pattern factor; R_{wp} : the weighted pattern factor.

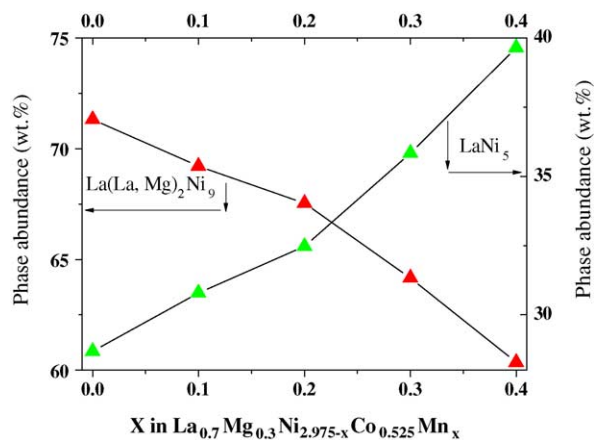


Fig. 3. Phase abundance of the $\text{La}(\text{La},\text{Mg})_2\text{Ni}_9$ phase and the LaNi_5 phase existing in the $\text{La}_{0.7}\text{Mg}_{0.3}\text{Ni}_{2.975-x}\text{Co}_{0.525}\text{Mn}_x$ ($x=0-0.4$) alloys.

above different results, which will inevitably influence the hydrogen storage and electrochemical characteristics of the alloys studied.

3.2. P - C isotherms

The electrochemical method is very useful for examining the charging and discharging levels of hydrogen in an anode, although the calculated pressures pertain to a quasi-equilibrium state. The P - C isotherms (PCT) of hydrogen desorption for hydrogenated $\text{La}_{0.7}\text{Mg}_{0.3}\text{Ni}_{2.975-x}\text{Co}_{0.525}\text{Mn}_x$ ($x=0, 0.1, 0.2, 0.3, 0.4$) compounds at 298 K are presented in Fig. 4. It should be noted that the partial substitution of Mn for Ni results in lower desorption pressure plateau and steeper pressure plateau of the alloy electrodes. In addition, we can find that, when x increases from 0 to 0.4, the hydrogen storage capacity first increases from 0.868 to 0.912 and then decreases to 0.836. This phenomenon is mainly ascribed to two reasons as follows: On the one hand, the plateau pressure decreases with increasing x , which enhances the intrinsic hydrogen storage capacity of alloys. On the other hand, as Oesterreicher et al. [11] has pointed out that the hydrogen

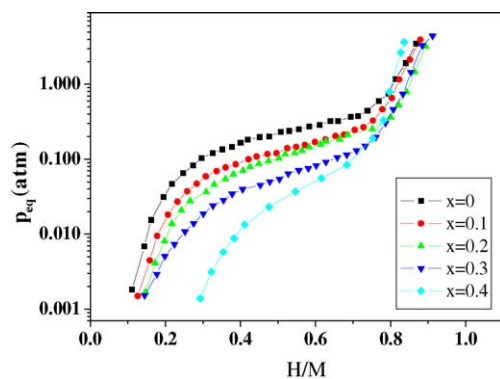


Fig. 4. The electrochemical P - C - T curves for $\text{La}_{0.7}\text{Mg}_{0.3}\text{Ni}_{2.975-x}\text{Co}_{0.525}\text{Mn}_x$ ($x=0-0.4$) alloy electrodes at 298 K.

storage capacity of the LaNi_3 phase is larger than that of the LaNi_5 phase. Moreover, as shown in Fig. 3 and Table 3, the $\text{La}(\text{La},\text{Mg})_2\text{Ni}_9$ phase abundance decreases while the LaNi_5 phase abundance increases with increasing x in alloys. The above contrary effects result in an optimum Mn content for the hydrogen storage capacity of the La-Mg-Ni-Co-Mn-type hydrogen storage alloys. The recommended amount of Mn addition is 0.3 from our work. Moreover, it is observed that there is only one plateau in each P - C - T curve of the alloy, as shown in Fig. 4. Since the unit cell of the AB_3 compounds contains one-third AB_5 structure and two-thirds AB_2 structure [7], it is perhaps concluded that the plateau pressure of the $\text{La}(\text{La},\text{Mg})_2\text{Ni}_9$ phase is similar to that of the LaNi_5 phase or the difference between their plateau pressures of AB_3 and AB_5 compounds is too small to be observed.

3.3. Activation and maximum discharge capacity

When hydrogen storage alloy electrode is first charged, the stored hydrogen in the alloy is released sparingly after absorption. The process that the freshly formed hydride electrodes are continuously charged and discharged in order to obtain the maximum electrochemical capacity is called activation. This is important for practical use of Ni-MH battery. Fig. 5 shows the activation profiles of the $\text{La}_{0.7}\text{Mg}_{0.3}\text{Ni}_{2.975-x}\text{Co}_{0.525}\text{Mn}_x$ ($x=0-0.4$) alloy electrodes, and the electrochemical characteristics are summarized in Table 4. It can be seen that all the alloys can be easily activated to reach their maximum capacity within two cycles, which means that activation of La-Mg-Ni-Co-Mn alloy electrodes is easy. With the increase of x , the maximum discharge capacity of the alloy electrode first increases from 337.6 mAh g^{-1} ($x=0$) to 356 mAh g^{-1} ($x=0.3$) and then decreases to 326.6 mAh g^{-1} ($x=0.4$), which is in good agreement with the results of P - C - T curves measurement mentioned above. The cycling capacity retention rate, expressed as $S_{70} (\%) = C_{70}/C_{\text{max}} \times 100$ (where C_{max} is the maximum discharge capacity, C_{70} is the discharge capacity at the 70th cycles) is also listed in Table 4. It is found that S_{70} is not changed obviously ($S_{70} = 50.2-49.6\%$) with increasing Mn content. In fact, the cycle stability of the alloy

Table 4
Summary of the electrode performance of $\text{La}_{0.7}\text{Mg}_{0.3}\text{Ni}_{2.975-x}\text{Co}_{0.525}\text{Mn}_x$ ($x=0-0.4$) alloy electrodes

Alloys	H/M	C_{max} (mAh g^{-1})	N_{a} ^a	HRC ₁₂₀₀ ^b (%)	HRD ₁₂₀₀ ^c (%)	S_{70} (%)
$x=0.0$	0.868	337.6	2	79	64.4	50.2
$x=0.1$	0.879	342.2	1	81.2	68.5	50.1
$x=0.2$	0.894	348.7	1	85.3	74.3	49.9
$x=0.3$	0.912	356.0	1	89.7	81.5	49.7
$x=0.4$	0.836	326.6	1	82.5	70.7	49.6

^a The cycle numbers needed to activate the electrodes.

^b The high rate chargeability at the discharge current density of 1200 mA g^{-1} .

^c The high rate dischargeability at the discharge current density of 1200 mA g^{-1} .

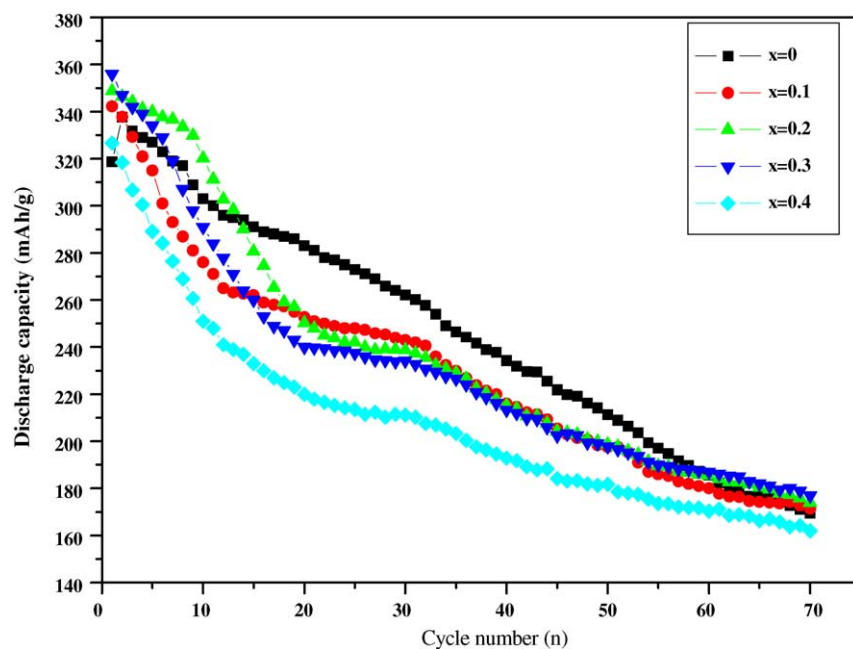


Fig. 5. The cycle life curves of the $\text{La}_{0.7}\text{Mg}_{0.3}\text{Ni}_{2.975-x}\text{Co}_{0.525}\text{Mn}_x$ ($x=0-0.4$) alloy electrodes at 298 K.

electrodes is decreased slightly with increasing x . Although the existence of Co would effectively prevent the corrosion of Mn in La–Mg–Ni–Co–Mn system alloys [35], the effect become weaker because of too much Mn addition in the alloy electrodes with increasing x . In spite of the improved electrochemical capacity of La–Mg–Ni–Co–Mn system alloys electrodes, their cycling stability is rather poor and hence has to be upgraded for practical applications.

3.4. High rate chargeability and dischargeability

It is very important to restrain the decrease of the discharge capacity even at the high charge/discharge current density for practical application of hydride electrode in Ni–MH battery. The dependence of discharge capacity of the $\text{La}_{0.7}\text{Mg}_{0.3}\text{Ni}_{2.975-x}\text{Co}_{0.525}\text{Mn}_x$ ($x=0-0.4$) alloy electrodes on current density is shown in Fig. 6. The HRC and HRD of the alloy electrodes at 1200 mA g^{-1} current density are also listed in Table 4. As expected, the HRC and HRD (taking the discharge capacity at charging/discharging rate of 60 mA g^{-1} as unity) of all the alloy electrodes decays with increasing current density. Nevertheless, the $\text{La}_{0.7}\text{Mg}_{0.3}\text{Ni}_{2.675}\text{Co}_{0.525}\text{Mn}_{0.3}$ alloy electrode shows the most satisfactory HRC and HRD than that of the other alloy electrodes. Taking the current density being 1200 mA g^{-1} as an example, the HRC of the alloy electrodes increases from 79% ($x=0$) to 89.7% ($x=0.3$) and then decreases to 82.5% ($x=0.4$), and the HRD of the alloy electrodes increases from 64.4% ($x=0$) to 81.5% ($x=0.3$) and then decreases to 70.7% ($x=0.4$). Those characteristic are quite different to Pan et al.'s results [33]. They pointed out that HRD of the alloy electrodes first increases from 66.7% ($x=0.0$) to 70.2% ($x=0.1$)

and then decreases to 50.0% with further increase of x . The HRD of the alloy electrodes in their paper are worse than that in our paper. The better HRD can be attributed to two reasons: on the one hand, the LaNi_5 phase works not only as a hydrogen reservoir but also as a catalyst to activate the $\text{La}(\text{La},\text{Mg})_2\text{Ni}_9$ phase to absorb/desorb reversibly hydrogen in the alkaline electrolyte [34]; on the other hand, as Meli et al. [36] has pointed out that when Ni is partially substituted by Mn in rare earth-based hydrogen storage alloys, the dissolution of Mn into electrolyte leads to the increase of Ni content on the alloy surface, which has good electrochemical catalytic property to improve the reaction rate of hydrogen. With increase of Mn content in the alloys, the LaNi_5 phase

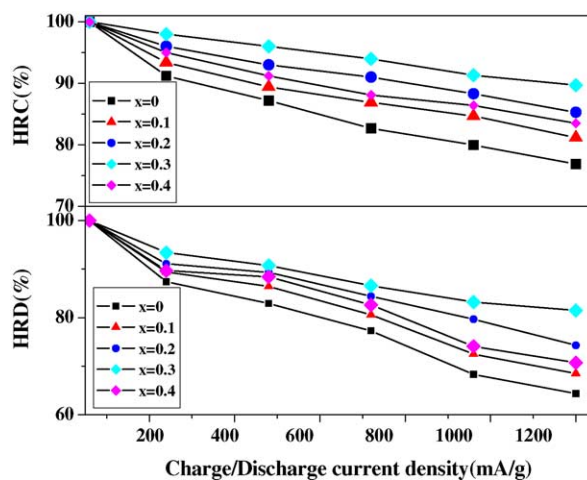


Fig. 6. The HRC and HRD of the $\text{La}_{0.7}\text{Mg}_{0.3}\text{Ni}_{2.975-x}\text{Co}_{0.525}\text{Mn}_x$ ($x=0-0.4$) alloy electrodes.

Table 5

The electrochemical kinetic parameters of $\text{La}_{0.7}\text{Mg}_{0.3}\text{Ni}_{2.975-x}\text{Co}_{0.525}\text{Mn}_x$ ($x=0-0.4$) alloy electrodes

Samples	Polarization resistance, R_p ($\text{m}\Omega$)		Exchange current density, I_0 (mA g^{-1})		Hydrogen diffusion coefficient, D ($\times 10^{-10} \text{ cm}^2 \text{ s}^{-1}$)	
	298 K	233 K	298 K	233 K	298 K	233 K
$x=0$	130.6	466.3	198.7	43.0	14.4	0.9
$x=0.1$	124.1	461.5	209.1	43.6	14.5	1.7
$x=0.2$	107.2	459.4	242.1	43.8	14.6	2.1
$x=0.3$	94.6	455.6	274.0	44.1	14.8	2.7
$x=0.4$	117.3	454.0	221.2	44.1	15.0	3.5

abundance increases, this is beneficial to the HRD. However, the total Ni content decreases, which are detrimental to the HRD. Those two contrary factors will result in an optimum Mn content in the alloys. Moreover, we can find that the LaNi_5 phase abundance in present paper is much than that in Pan et al.'s study, which will reasonably lead to higher HRD. It is generally accepted that the HRC and HRD of metal hydride electrode are influenced mainly by the electrochemical reaction kinetics on the alloy surface and the diffusion rate of hydrogen in the bulk of the alloy [34]. To examine the effect of the partial substitution of Mn for Ni on the charge and discharge kinetics, linear polarization is performed on these alloy electrodes. Based on the measured linear polarization curves, values of exchange current density I_0 and polarization resistance R_p was evaluated for the alloy electrodes and are summarized in Table 5. Fig. 7 shows the HRC and HRD as a function of the exchange current density, I_0 , for hydrogen evolution reaction of the alloy electrodes. The HRC and HRD show a linear relationship with the exchange density for the electrodes. Moreover, we can find that the hydrogen diffusion coefficient almost unchanged ($14.4-15.0 \times 10^{-10} \text{ cm}^2 \text{ s}^{-1}$). Iwakura et al. [37] have shown that if the electrochemical reaction on the surface is the rate-determining factor, a linear dependence of the high rate dischargeability on the exchange current density should be observed. In contrast, if the diffusion of hydrogen in the bulk is the rate-determining factor, the high rate chargeability/dischargeability should be constant, irrespective of exchange density. Therefore, in the

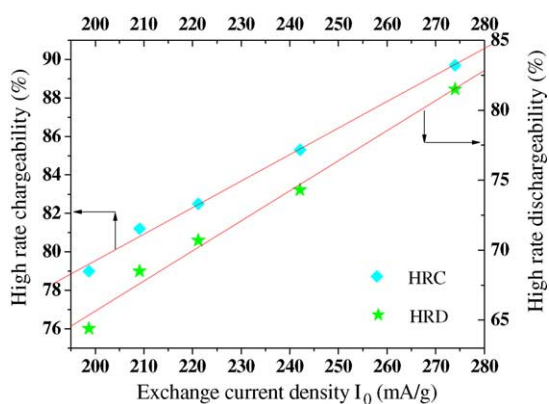


Fig. 7. HRC and HRD at 1200 mA g^{-1} of $\text{La}_{0.7}\text{Mg}_{0.3}\text{Ni}_{2.975-x}\text{Co}_{0.525}\text{Mn}_x$ ($x=0-0.4$) alloy electrodes as a function of exchange current density.

present study, the HRC and HRD are essentially controlled by the charge-transfer reaction of hydrogen on the surface at a discharge current density of 1200 mA g^{-1} .

3.5. Low-temperature dischargeability (LTD)

It has been reported that the discharge capacity of the negative electrode in nickel–metal hydride decrease drastically with decreasing temperature [38]. Sakai et al. has [2] pointed out that the dischargeability of the negative electrodes at relative low temperature depended on the hydrogen diffusion and/or charge-transfer process occurring at the metal electrolyte interface. The hydrogen diffusion coefficient (D) of hydrogen in the bulk is evaluated using the method described by Iwakura et al. [39]. The LTD, expressed as $\text{LTD}_{233} (\%) = C_{233}/C_{298} \times 100$ (where C_{233} and C_{298} are the discharge capacity at 233 and 298 K, respectively). The D and I_0 of the $\text{La}_{0.7}\text{Mg}_{0.3}\text{Ni}_{2.975-x}\text{Co}_{0.525}\text{Mn}_x$ ($x=0, 0.1, 0.2, 0.3, 0.4$) alloy electrodes at 233 K are also listed in Table 5, respectively. It can be found that both the I_0 and the D are smaller than that at 298 K. Moreover, we can find that the I_0 maintain almost unchanged ($43.0-44.1 \text{ mA g}^{-1}$), whereas the D increases remarkably with increasing x , which implies that the hydrogen diffusion in alloy probably becomes the rate-determining factor for low-temperature dischargeability at 233 K. Zhao et al. [40] thought that desorption of hydrogen in metal hydride is an endothermal

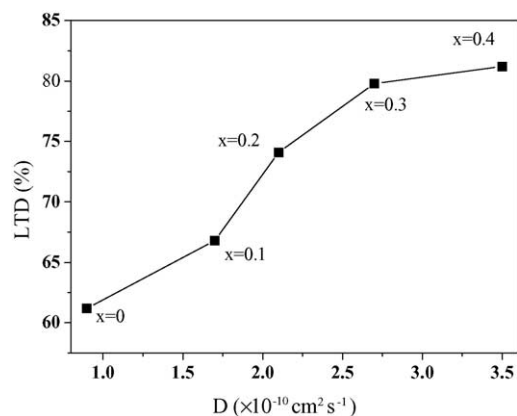


Fig. 8. The low-temperature dischargeability (LTD) as a function of hydrogen diffusion coefficient (D) of the $\text{La}_{0.7}\text{Mg}_{0.3}\text{Ni}_{2.975-x}\text{Co}_{0.525}\text{Mn}_x$ ($x=0, 0.1, 0.2, 0.3, 0.4$) alloy electrodes at 233 K.

reaction and may be a rate-limiting step during the discharge process of metal hydride at relatively low temperature (for example, at 233 K). Fig. 8 shows the LTD as a function of D in the alloy electrodes. It can be easily found that the D increases with the increase of x , which can be attributed to the cell volume expansion with increasing x as shown in Table 3. The larger D , the larger LTD of the alloy electrodes.

4. Conclusion

The effects of Mn content on the structure and the electrochemical characteristics of $\text{La}_{0.7}\text{Mg}_{0.3}\text{Ni}_{2.975-x}\text{Co}_{0.525}\text{Mn}_x$ ($x=0, 0.1, 0.2, 0.3, 0.4$) hydrogen storage alloys are investigated systematically. It is found by XRD Rietveld analysis that all these alloys mainly consist of two phases: the $\text{La}(\text{La},\text{Mg})_2\text{Ni}_9$ phase with the rhombohedral PuNi_3 -type structure and the LaNi_5 phase with the hexagonal CaCu_5 -type structure. P - C - T curves reveal that the plateau pressure decreases progressively and the hydrogen storage capacity increases first and then decreases with increasing Mn content in the alloys. The electrochemical measurements show that the maximum discharge capacity of the alloy electrode increases first from 337.6 mAh g^{-1} ($x=0$) to 356 mAh g^{-1} ($x=0.3$) and then decreases to 326.6 mAh g^{-1} ($x=0.4$). For a discharge current density of 1200 mA g^{-1} , the HRC of the alloy electrodes increases from 79% ($x=0$) to 89.7% ($x=0.3$) and then decreases to 82.5% ($x=0.4$), and the HRD of the alloy electrodes increases from 64.4% ($x=0$) to 81.5% ($x=0.3$) and then decreases to 70.7% ($x=0.4$). Linear polarization shows that the exchange current density I_0 first increases from 198.7 mA g^{-1} ($x=0$) to 274.0 mA g^{-1} ($x=0.3$) and then decreases to 221.2 mA g^{-1} ($x=0.4$) with increasing Mn content, which suggests that the electrochemical kinetics of the alloy electrodes first increase and then decrease when Ni is partially substituted by Mn in the alloys. The D increases with increasing Mn content and thus increases the low temperature dischargeability LTD of the alloy electrodes.

Acknowledgement

This work was financially supported by the National Natural Science Foundation of China (Grant No. 20171042).

References

- [1] M. Latroche, A. Percheron-Guegan, *J. Alloys Compd.* 356–357 (2003) 461.
- [2] J.J.G. Willems, K.H.J. Buschow, *J. Less-Common Met.* 129 (1987) 13.
- [3] T. Sakai, H. Miyamura, N. Kuriyama, A. Kato, K. Oguro, H. Ishikawa, *J. Electrochem. Soc.* 137 (1990) 795.
- [4] T. Kohno, H. Yoshida, F. Kawashima, T. Inaba, I. Sakai, M. Yamamoto, M. Kanda, *J. Alloys Compd.* 311 (2000) L5.
- [5] J.J.G. Willems, *Philips J. Res.* 39 (Suppl. 1) (1984) 1.
- [6] H.G. Pan, Y.F. Zhu, M.X. Gao, Q.D. Wang, *J. Electrochem. Soc.* 149 (2002) A829.
- [7] J. Chen, N. Kuriyama, H.T. Takeshita, H. Tanaka, T. Sakai, M. Haruta, *Electrochem. Solid-State Lett.* 3 (6) (2000) 249.
- [8] H. Ogawa, M. Ikoma, H. Kawano, I. Matsumoto, *J. Power Sources* 12 (1988) 393.
- [9] S.R. Ovshinsky, M.A. Fetcenko, *J. Ross. Sci.* 260 (1993) 176.
- [10] J.J. Reilly, in: J.O. Besenhard (Ed.), *Handbook of Battery Materials*, Wiley, New York, 2000.
- [11] H. Oesterreicher, J. Clinton, H. Bittner, *Mater. Res. Bull.* 11 (1976) 1241.
- [12] H. Oesterreicher, K. Ensslen, A. Kerlin, E. Bucher, *Mater. Res. Bull.* 15 (1980) 275.
- [13] K. Kadir, T. Sakai, I. Uahara, *J. Alloys Compd.* 257 (1997) 115.
- [14] K. Kadir, N. Nuriyama, T. Sakai, I. Uehara, L. Eriksson, *J. Alloys Compd.* 284 (1999) 145.
- [15] K. Kadir, T. Sakai, I. Uahara, *J. Alloys Compd.* 287 (1999) 264.
- [16] K. Kadir, T. Sakai, I. Uahara, *J. Alloys Compd.* 302 (2000) 112.
- [17] J. Chen, H.T. Takeshita, H. Tanaka, N. Kuriyama, T. Sakai, *J. Alloys Compd.* 302 (2000) 304.
- [18] H.G. Pan, Y.F. Liu, M.X. Gao, Y.F. Zhu, Y.Q. Lei, Q.D. Wang, *J. Alloys Compd.* 351 (2003) 228.
- [19] J.M. Wu, J. Li, W.P. Zhang, F.J. Muo, L.C. Tai, R.G. Xu, *J. Alloys Compd.* 248 (1997) 180.
- [20] P.H.L. Notten, M. Latroche, A. Percheron-Guegan, *J. Electrochem. Soc.* 146 (9) (1999) 3181.
- [21] W.E. Wallace, F. Pourarlan, *J. Phys. Chem.* 86 (1982) 4958.
- [22] J.X. Ma, H.G. Pan, C.P. Chen, Q.D. Wang, *J. Alloys Compd.* 343 (2002) 164.
- [23] A. Apostolov, N. Stanev, P. Tcholakov, *J. Less-Common Met.* 110 (1985) 127.
- [24] C. Lartigue, A. Percheron-Guégan, J.C. Achard, *J. Less-Common Met.* 75 (1980) 23.
- [25] J.J. Reilly, G.D. Adzic, J.R. Johnson, T. Vogt, S. Mukerjee, J. McBreen, *J. Alloys Compd.* 293–295 (1999) 569.
- [26] T. Sakai, K. Oguro, H. Miyamura, A. Kato, H. Ishikawa, *J. Less-Common Met.* 161 (1990) 193.
- [27] H. Ogawa, M. Ikoma, *J. Power Sources* 12 (1998) 393.
- [28] A. Percheron-Guégan, C. Lartigue, J.C. Achard, *J. Less-Common Met.* 109 (1985) 287.
- [29] C.J. Howard, *J. Appl. Cryst.* 15 (1982) 615.
- [30] X.B. Zhang, Y.J. Chai, W.Y. Yin, M.S. Zhao, *J. Solid State Chem.* 177 (2004) 2373.
- [31] D.N. Gruen, M.H. Mendelsohn, A.E. Dwight, *J. Less-Common Met.* 161 (1977) 193.
- [32] H.G. Pan, Q.W. Jin, M.X. Gao, Y.F. Liu, R. Li, Y.Q. Lei, *J. Alloys Compd.* 373 (2004) 237.
- [33] H.G. Pan, Y.F. Liu, M.X. Gao, Y.F. Zhu, Y. Lei, Q. Wang, *J. Electrochem. Soc.* 151 (2004) A374.
- [34] H.G. Pan, Y.F. Liu, M.X. Gao, Y.Q. Lei, Q.D. Wang, *J. Electrochem. Soc.* 150 (5) (2003) A565.
- [35] Y.F. Liu, H.G. Pan, M.X. Gao, Y.F. Zhu, Y.Q. Lei, Q.D. Wang, *Int. J. Hydrogen Energy* 29 (2004) 297.
- [36] F. Meli, A. Zuttel, L. Schlabach, *J. Alloys Compd.* 202 (1993) 81.
- [37] C. Iwakura, T. Oura, H. Inoue, M. Matsuoka, *Electrochim. Acta* 41 (1996) 117.
- [38] H. Senoh, Y. Hara, H. Inoue, C. Iwakura, *Electrochim. Acta* 46 (2001) 967.
- [39] C. Iwakura, H. Senoh, K. Morimoto, Y. Hara, H. Inoue, *Electrochemistry* 70 (1) (2002) 2.
- [40] M. Zhao, C. Sun, in: T. Nejet Veziroglu, et al. (Eds.), *II. Materials, Physics and Chemistry*, vol. 82, Kluwer Academic Publisher, 2002, p. 29.